Optica Applicata, Vol. LII, No. 3, 2022
DOI: 10.37190/oa220310

Polarization dependent high refractive index metamaterial with metallic dielectric grating structure in infrared band

Jianmin Li[1], Peng Chen[2], Bo Fang[2,*], Jinhui Cai[2], Le Zhang[2], Yinglai Wu[3], Xufeng Jing[4,5,&]

[1]University of Shanghai for Science and Technology,
No.516 JungGong Road, Shanghai 200093, China

[2]College of Metrology & Measurement Engineering, China Jiliang University,
Hangzhou 310018, China

[3]School of Entrepreneurship, Hangzhou Dianzi University, Hangzhou 310000, China

[4]Institute of Optoelectronic Technology, China Jiliang University, Hangzhou 310018, China

[5]Centre for THz Research, China Jiliang University, Hangzhou 310018, China

Corresponding authors: [*]fangbo@cjlu.edu.cn, [&]jingxufeng@cjlu.edu.cn

According to the theory of high refractive index of metamaterials, a composite structure of metal dielectric grating was designed to achieve high refractive index in infrared band. Based on the *S*-parameter inversion algorithm, we extracted the effective permittivity, the effective permeability, and the effective refractive index of the designed metamaterial. By changing the geometric parameters of the composite grating metamaterial structure, the effective refractive index of the designed metamaterial reaches more than 8.0 at the infrared resonance frequency. This is a high refractive index that many natural materials cannot achieve. It is noteworthy that the metamaterial structure has obvious polarization sensitivity. The metamaterial structure has both high refractive index and wideband zero refractive index properties when different polarized light is incident. At the same time, we further investigate the influence of metamaterial geometric parameters on the effective refractive index of metamaterials. Also, we propose a double grating metamaterial structure to obtain more degrees of freedom of metamaterial on the effective refractive index.

Keywords: metamaterials, high refractive index, infrared band.

1. Introduction

Metamaterials refer to composites with artificially designed structures that exhibit extraordinary physical properties not found in natural materials [1–10]. They have some special properties, such as allowing light and electromagnetic waves to change their

usual properties. This effect is not possible with traditional materials [11–20]. Metamaterials have promising application prospects in super resolution imaging, perfect absorption, hyperlens, electromagnetic cloaking technology, *etc*. [21–30]. Metamaterials are able to achieve abnormal physical properties mainly because they can achieve different equivalent material parameters, such as negative refractive index, zero refractive index and high refractive index [31–38]. At present, most studies on metamaterials are focused on negative index metamaterials and zero index metamaterials, and relatively few studies on high index metamaterials.

High refractive index metamaterials have promising applications in microscopic imaging and slow light devices. The refractive index of materials will largely restrict the imaging resolution, and the design and preparation of material with high refractive index properties can greatly improve the imaging resolution [39]. In addition, high refractive index materials in the broadband domain can induce slow light effects, and the design and preparation of a high refractive index metamaterial can enhance the storage capacity of delay lines and spectral sensitivity of the interferometer [40]. In nature, the refractive index of materials is generally a relatively small value, and only a few semiconductor materials and insulators, for example, lead sulfide and strontium titanate, will show a peak refractive index in mid-infrared and far-infrared bands. Based on metamaterial technology, the equivalent parameters of materials can be controlled artificially, and it is possible to design a material with high refractive index using metamaterial [41-45].

Here, based on polarization-sensitive metal grating structure, we propose a metal -dielectric hybrid metamaterial in the infrared band. The metamaterials have different equivalent refractive index under different incident polarization conditions, and achieve high refractive index characteristics of polarization sensitivity. By changing the size of the spacing between the grating strips, the high refractive index properties of the metamaterial change accordingly. We further propose a double grating structure metamaterial. Notably, this dual grating metamaterial can achieve broadband zero-refractive index properties.

2. Principle of high refractive index metamaterials

According to the effective refractive index $n = \sqrt{\varepsilon_r \mu_r}$, it can be seen that the refractive index of a material is determined by its dielectric constant and its permeability. In order to increase the equivalent refractive index, we can increase the equivalent dielectric constant and the equivalent permeability. The effective permittivity can be expressed as

$$\varepsilon = 1 + \frac{P}{\varepsilon_0 E} \tag{1}$$

where P is the polarization and ε_0 is the permittivity in free space. It is known that the polarization can be infuenced by the dipolar interaction between the parallel plate capacitors. The capacitor can generate the accumulation effect of charges in gap, and

the charges can result in a significant dipole moment to enhance the effective permittivity [46]. Also, the effective permeability can be described as

$$\mu = 1 + M/H \tag{2}$$

where M indicates magnetization. The strong diamagnetic response will also influence the effective index. SHIN *et al.* [47] demonstrated that the diamagnetic effect resulted from the magnetic moments reduced by surface currents, and the strength of magnetic dipole moment was proportional to the area subtended by the current loops. Therefore, we can reduce the diamagnetic effect to enhance the effective permeability. Therefore, the effective refractive index of metamaterials should be dependent on the different aspects of geometric structure.

Recently, the parallel line charge accumulation model was proposed by CHOI *et al*. to evaluate the effective refractive index of metamaterials [48]. The gap width between unit cells of metamaterial can be defined as g. When g is much smaller than the metamaterial unit structure size, $g \ll L$, the strong coupled capacitor can be generated. The accumulated charges between capacitor can be described by

$$Q \propto \varepsilon_0 \varepsilon_\mathrm{p} \frac{L^3}{g} E_\mathrm{in} \tag{3}$$

where ε_p is the relative permittivity of the substrate material, and E_in indicates the incident electric field. The effective permittivity of metamaterials can be calculated as

$$\varepsilon_\mathrm{r} = \varepsilon_\mathrm{p} + \frac{P}{\varepsilon_0 E} \tag{4}$$

In Eq. (4), $E = (L/g)^{\beta} E_\mathrm{in}$, where β is a dimensionless fitting parameter, and the polarization density P can be evaluated by

$$P = \frac{Q(L-g)}{L^2 d} \tag{5}$$

According to Eq. (3), it can be seen that the gap widths between cell structures are inversely proportional to the cumulative charge. We can increase the accumulated charge by reducing the gap between the metamaterial unit structures. According to Eq. (4) and Eq. (5), the dipole momentum is directly proportional to the cumulative charge between the capacitors, and we can increase the cumulative charge to increase the metamaterial's equivalent dielectric constant. At the same time, we can reduce the thickness of the metal unit structure to reduce the diamagnetic effect, thus improving the metamaterial's equivalent permeability.

3. Metamaterials effective parameter extraction method

Generally, the standard S-parameter inversion method can be applied to calculate the effective refractive index of metamaterials [49, 50]. The metamaterial structure can be

regarded as an equivalent uniform plate, and the equivalent basic parameters of the metamaterial structure can be inversely calculated from the transmission and reflection coefficients of the equivalent plate. The *S*-parameter for a uniform plate of metamaterial with thickness d can be described as

$$S_{11} = \frac{R_{01}[1 - \exp(i2nk_0d)]}{1 - R_{01}^2 \exp(i2nk_0d)} \tag{6}$$

$$S_{21} = \frac{(1 - R_{01}^2)\exp(i2nk_0d)}{1 - R_{01}^2 \exp(i2nk_0d)} \tag{7}$$

where S_{11} and S_{21} are the reflection coefficient and transmission coefficient, respectively, n is the effective refractive index, d is the effective thickness of the metamaterial, k is the wave number of the incident wave, and R_{01} is the half-space reflection coefficient, and $R_{01} = (Z - 1)/(Z + 1)$. Z is the surface impedance of metamaterials.

According to the inversion method, we can obtain the effective material parameters of metamaterials as

$$z = \pm\sqrt{\frac{(1 + S_{11})^2 - S_{21}^2}{(1 - S_{11})^2 - S_{21}^2}} \tag{8}$$

$$\exp(ink_0d) = \frac{S_{21}}{1 - S_{11}\dfrac{z - 1}{z + 1}} \tag{9}$$

$$n = \frac{1}{k_0 d}\left\{\left\{\left[\ln[\exp(ink_0d)]\right]'' + 2m\pi\right\} - i\left[\ln[\exp(ink_0d)]\right]'\right\} \tag{10}$$

Here, $(\cdot)''$ represents the real part of a certain complex number parameter, and $(\cdot)''$ represents the imaginary part of a certain complex number parameter. Generally, $z'' \geq 0$, $n'' \leq 0$ for a passive material. In Eq.(10), m is the branch of the real part of the refractive index n, and m can be defined as $m = 1$. Thus, the effective impedance z and effective refractive index n of a metamaterial can be evaluated by Eq. (8) and Eq. (10), and the effective permittivity and effective permeability can be calculated by $\varepsilon = n/z$ and $\mu = nz$.

4. Design of polarization-sensitive high refractive index metamaterials

In order to achieve high refractive index metamaterials, we propose a periodically arranged dielectric metal grating structure as shown in Fig. 1. The metamaterial structure is made up of thin layers that are symmetrical above and below with metallic lines in between. The base medium material is silica, and the metal material is gold. After pre-

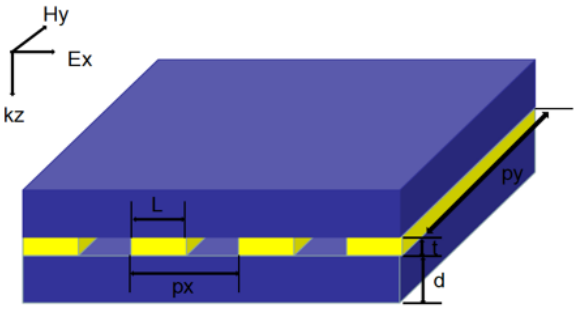

Fig. 1. Schematic diagram of dielectric metal grating composite metamaterial structure.

liminary optimization, we obtained that the grating period Px is 400 nm, the substrate thickness *d* is 40 nm, the metal thickness *t* is 20 nm, and the metal wire width *l* is 300nm. We define the gap between the metal lines as *g*, and *g* = 100 nm.

When the light vector of the light wave is perpendicular to the grating bar (TM mode) with normal incidence, we can calculate the *S* parameters of the metamaterial structure based on the finite integral method as shown in Fig. 2. Figure 2**a** shows the transmission and reflection coefficient from 150 to 750 THz (400–2000 nm wavelength). The corresponding phase is shown in Fig. 2**b**. It can be seen that significant electromagnetic resonance occurs around 300 THz. In the numerical simulation, the finite integral method was applied to calculate optical characteristics of unit cells. The unit cell boundary was used in the *x* and *y* directions. The open boundary was applied in the *z* direction. The near-field distributions of the designed metamaterial were numer-

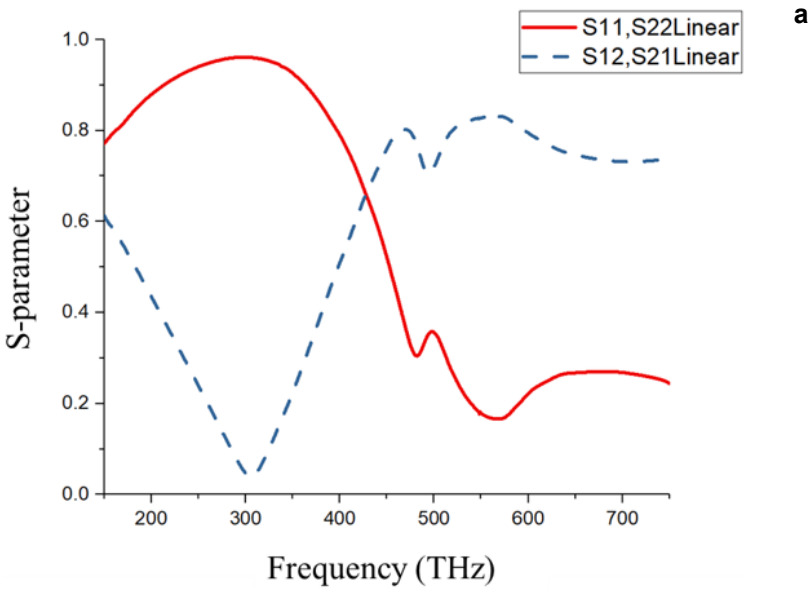

Fig. 2. (**a**) *S*-parameter of metamaterial, (**b**) phase of transmission and reflection.

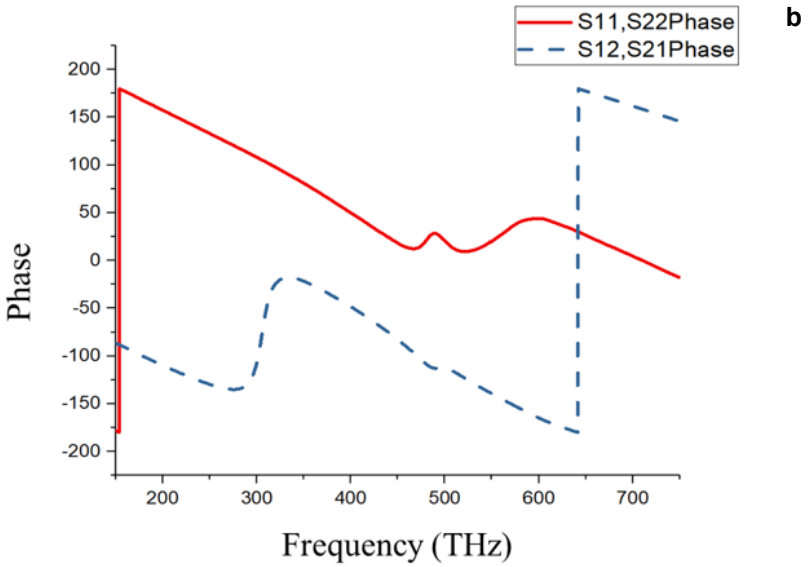

Fig. 2. Continued.

ically simulated using the finite integral method. All the models described in our work were meshed using triangular elements with a maximum size of one-twentieth the wavelength.

According to *S*-parameter inversion method, we can extract the effective parameters of the designed metamaterial as shown in Fig. 3. Figure 3**a** shows the effective per-

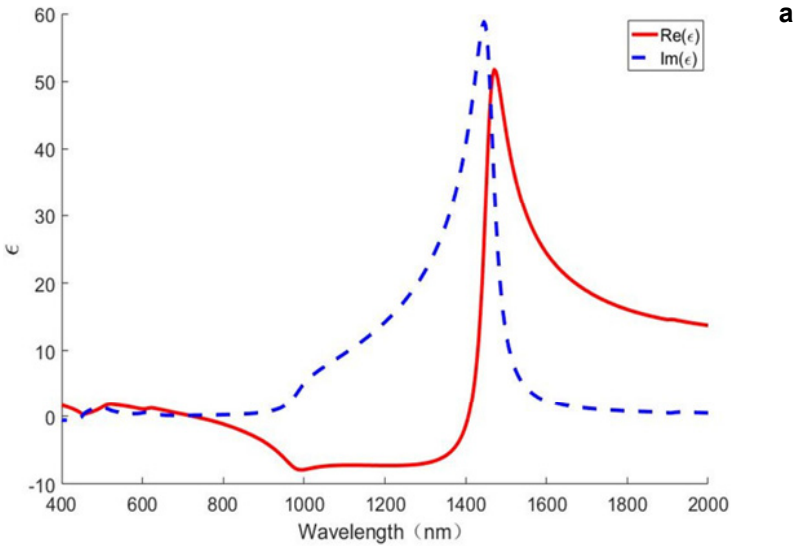

Fig. 3. (**a**) The calculated effective permittivity of metamaterial, (**b**) the effective permeability, (**c**) the effective refractive index.

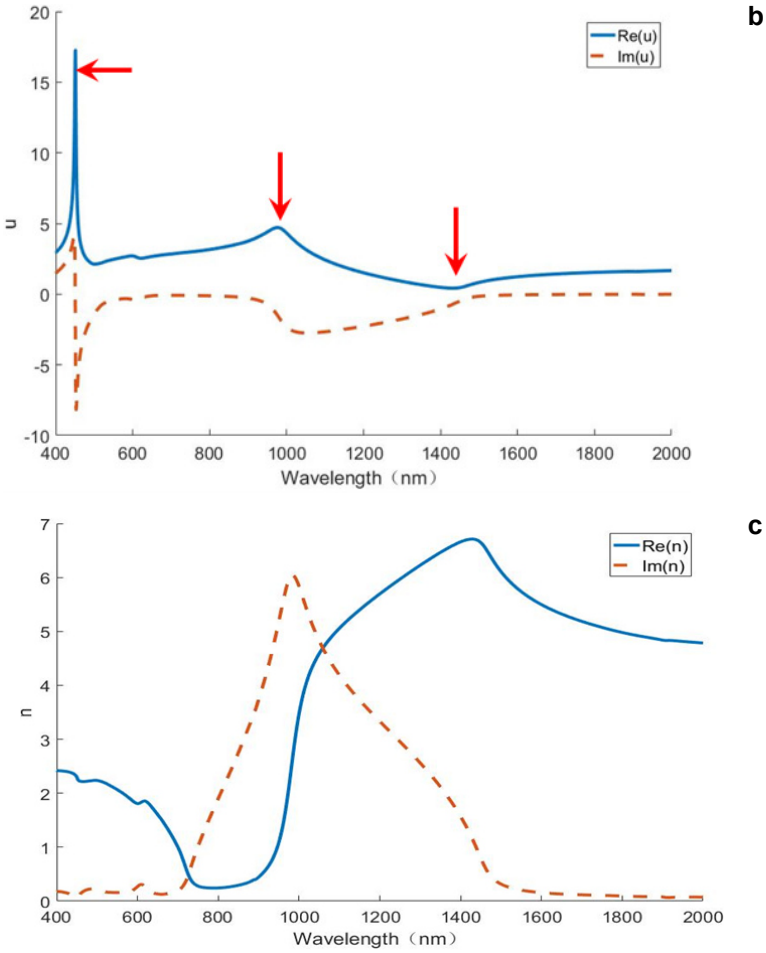

Fig. 3. Continued.

mittivity of designed metamaterial. It can be seen that a high peak occurs at about 1500 nm, and the effective dielectric constant of this peak is about 52. When the light wave is incident into designed metamaterial, the gap between the two grating bars can be regarded as a capacitor. At the resonant frequency, a large amount of charge accumulates between the metal gaps, which leads to the formation of a large electric dipole moment near the edge of the metal strips, leading to the increase of the effective dielectric constant. In Fig. 3**a**, the real part of the equivalent permittivity shows a broadband negative refractive index characteristic from 1000 to 1400 nm. With the increase of wavelength, the imaginary part of the equivalent permittivity increases gradually, and its value is positive. This wideband negative refractive index resonance may be attributed to the electrical dipole resonance of the metal grating structure.

Figure 3**b** shows the effective permeability of designed metamaterial. There is a smaller value at the resonant region of about 1450 nm, but the higher resonant peaks

for the effective permittivity occur with the effective permittivity of about 5. In Fig. 3**b**, the red arrow at the wavelength of 1450 nm shows the fundamental resonant mode, and the red arrow at the wavelength of about 1000 nm indicates the second-order resonant mode. The more higher order resonant mode is shown with the red arrow at about 450 nm. At the first order resonant position, the magnetic permeability is near zero. The peak of magnetic permeability in the visible region can reach about 17. This may be attributed to the diamagnetic effect with the permittivity near zero at the first order resonance. The occurrence of diamagnetic response causes a decrease in magnetic permeability. Although the effective permeability of the metamaterial is relatively small at the electric dipole resonance wavelength of 1450 due to the diamagnetic effect, this results in a large effective refractive index due to the strong electric dipole resonance. Figure 3**c** shows the effective refractive index of designed metamaterial. An unnaturally high refractive index with about 6.5 in the infrared region at about 1450 nm is revealed.

In order to further explain the physical mechanism of the high refractive index characteristics, we calculated the electric field distribution under the first order mode resonance condition at about 1450 nm as shown in Fig. 4. The strongly confined electric field is distributed in the gaps between grating bars. A large amount of charge accumulates between the strips, causing the dipole to gain momentum. We found that the direction of the induced electric field vector between the grating bars is opposite to the direction of the surface electric field vector because the TM mode incident light is perpendicular to the metamaterial structure. The intensity of electric field in the gap at the electric resonance is much stronger than that of incident field, which leads to the enhancement of the effective permittivity.

Next, we demonstrate the effect of different polarizations on the equivalent parameters of the designed metamaterials. Figure 5 shows the effective parameters of designed metamaterial with the optimization of geometric parameters. We define the TE mode as the direction of the electric field vector parallel to the grating bar. We keep

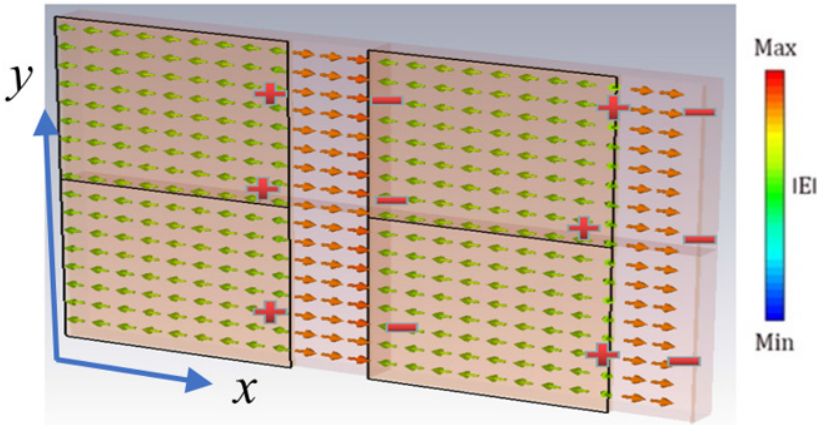

Fig. 4. Top view of the electric field distribution at the fundamental mode resonant frequency at 1450 nm.

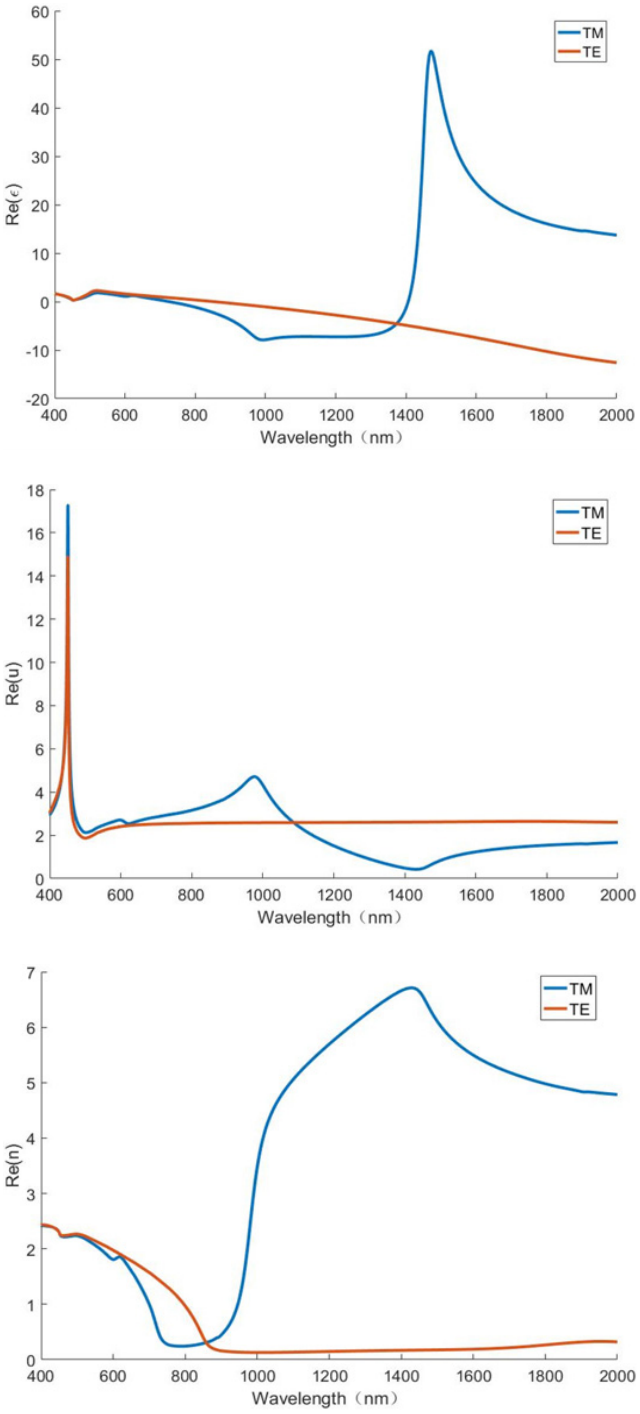

Fig. 5. Effect of different polarization on effective parameters. (**a**) The effective permittivity, (**b**) the effective permeability, (**c**) the effective refractive index.

the grating gap at 100 nm. As shown in Fig. 5**a** with the effective permittivity, when the incident light is in TE mode, the effective dielectric constant appears negative in the resonance region and the resonance property disappears. When the incident light is in TM mode, the effective dielectric constant is higher than 50 at the resonance wavelength of 1500 nm. Figure 5**b** shows the effective permeability with different polarization incidence. We find that when the incident light is in TE mode, both the first and second order modes of the permeability resonance disappear, and the position of the first order resonance mode coincides with that of the advanced mode resonance under TM incident condition. Figure 5**c** shows the effective refractive index of designed metamaterial. When the incident light wave is in TE mode, the broadband zero refractive index appears in the high refractive index region under the TM mode incident condition. So, for the metamaterial we designed, we can significantly change the effective refractive index of the metamaterial by changing the incident polarization state. In general, previous research has focused on designing metamaterials that have high or zero refractive index properties. Our metamaterials have both high and zero refractive indices with different polarization.

5. The influence of geometric parameters for the effective refractive index

Next, we will show the variation of the grating geometric parameters with respect to the equivalent refractive index, especially the grating strip gap width *g*. We keep the TM mode incident and the other geometric parameters unchanged. Figure 6 shows the effect of grating gap change on effective parameters. In Fig. 6**a**, with the decrease of gap *g*, the resonance wavelength appears red shift. The bandwidth of the negative re-

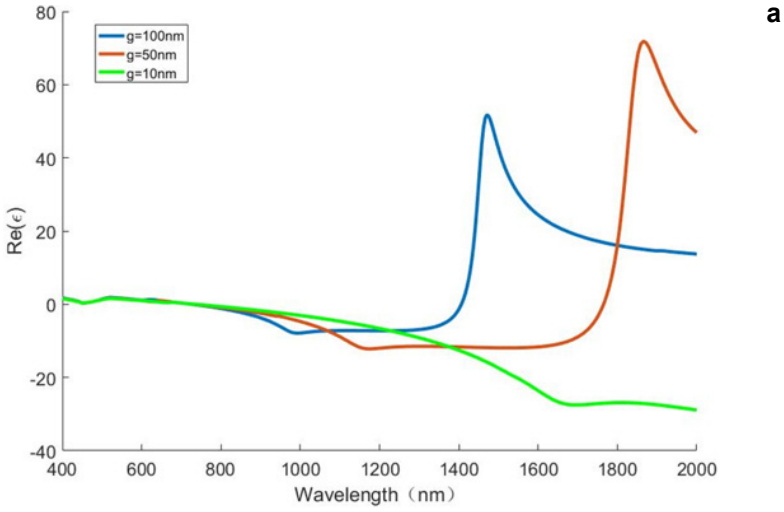

Fig. 6. Effect of grating gap change on effective parameters, (**a**) the effective permittivity, (**b**) the effective permeability, (**c**) the effective refractive index.

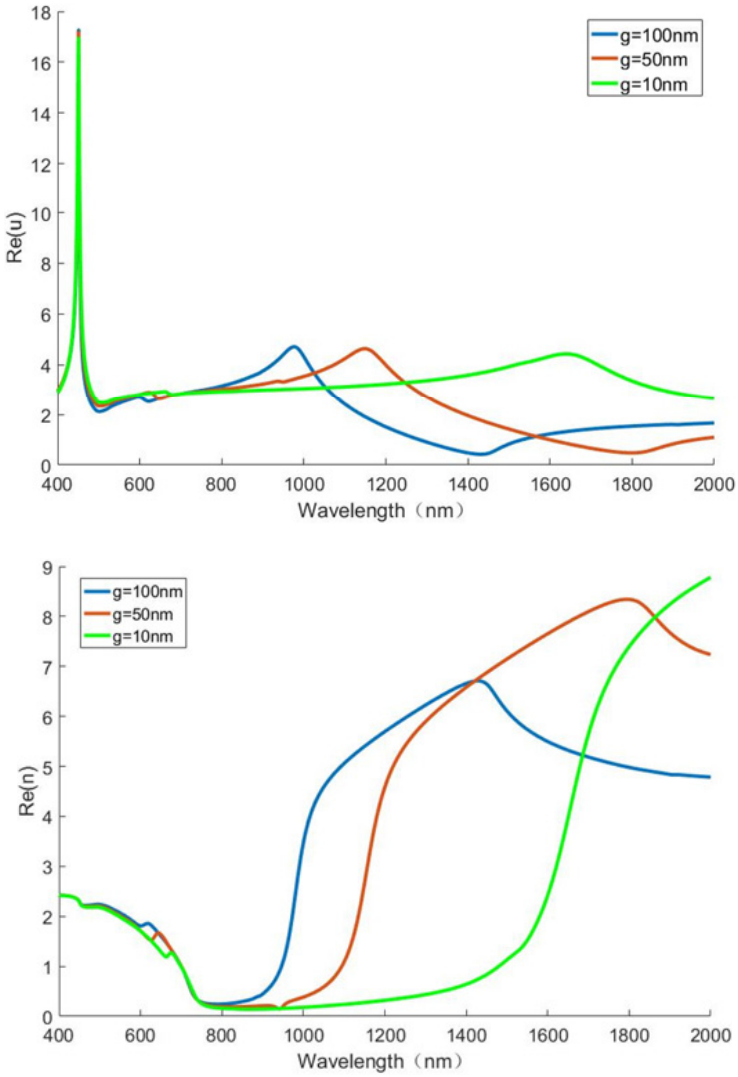

Fig. 6. Continued.

fractive index increases, and the absolute value of the negative refractive index increases. As g decreases, the maximum dielectric constant increases at the resonant frequency. Figure 6**b** shows the effective permeability with changing gap g. It is found that the first and second order resonance of the permeability is redshifted, but for the higher mode resonance, the resonant frequency does not change as g changes. Figure 6**c** indicates the effective refractive index with different gap width. When the gap width decreases, the resonant frequency of effective refractive index appears red shift and the resonant peak increases. When g = 10 nm, the phenomenon of broadband zero refractive index appears in the infrared band. In other words, we designed meta-

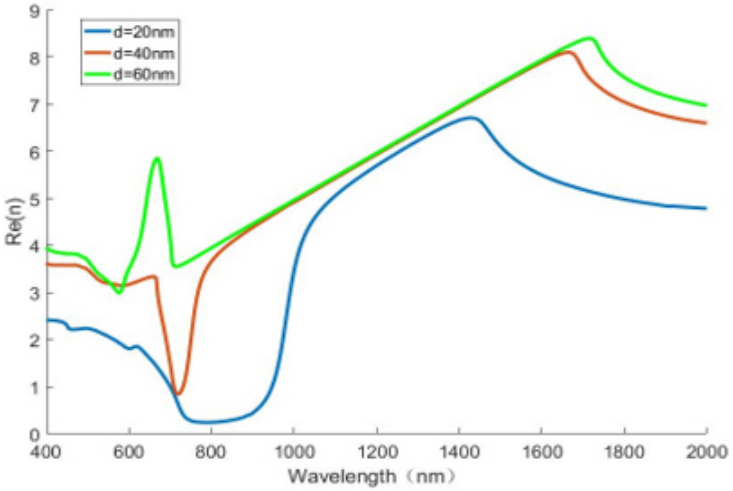

Fig. 7. Effect of metal thickness on effective refractive index.

materials that can achieve high and zero refractive index properties in different bands by changing the width of the gap.

Figure 7 indicates the effect of metal thickness on effective refractive index. We set g = 100 nm, other geometric parameters remain unchanged, and the polarization of incident light is TM mode. As can be seen, with the increasing of metal thickness d, the curve of refractive index keeps moving towards the direction of long wave. At the same time, the peak of refractive index obviously keeps increasing. This is because the increasing of metal thickness increases the amount of charge that can be held in it, leading to the continuous increase of refractive index. At the wavelength of 700 nm, there is a resonant effect of refractive index mutation at d = 40 nm and d = 60 nm. When d = 40 nm, the real part of the equivalent refractive index is reduced from 3 to 1. When d = 60 nm, the real part of the equivalent refractive index is increased from 3 to 6. This resonance phenomenon may be related to the accumulation of electric charge in the metal tank.

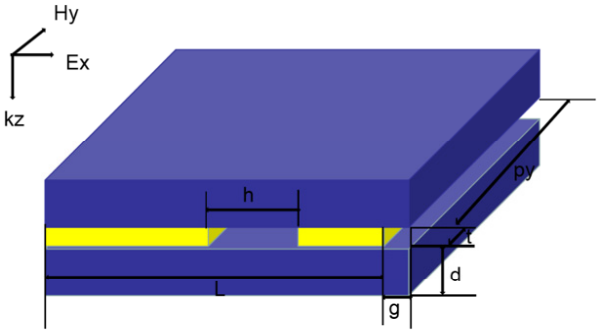

Fig. 8. Schematic diagram of double grating unit structure.

To further illustrate the effect of grating geometry parameters on the effective metamaterial parameters, we propose a double grating structure as shown in Fig. 8. Figure 8 shows the unit cell of the double grating structure. In other words, we split the original grating bar into two bars of unequal width. In a grating period, there are two grating strips of unequal width, thus we have double grating structure. The gap between two grating strips in a period can be considered as h. Also, the period of grating can be defined as Px = L + g. When g = 10 nm, h = 10 nm, Px = 400 nm, d = 40 nm, t = 20 nm, the extracted effective constitutive parameters are shown in Fig. 9 when the light is incident with TM mode. The comparison between the single grating structure and double grating structure on the effective constitutive parameters is given. Figure 9**a** indicates the effective permittivity of designed metamaterials. It can be seen that the double grating structure shows larger negative refractive index in absolute value

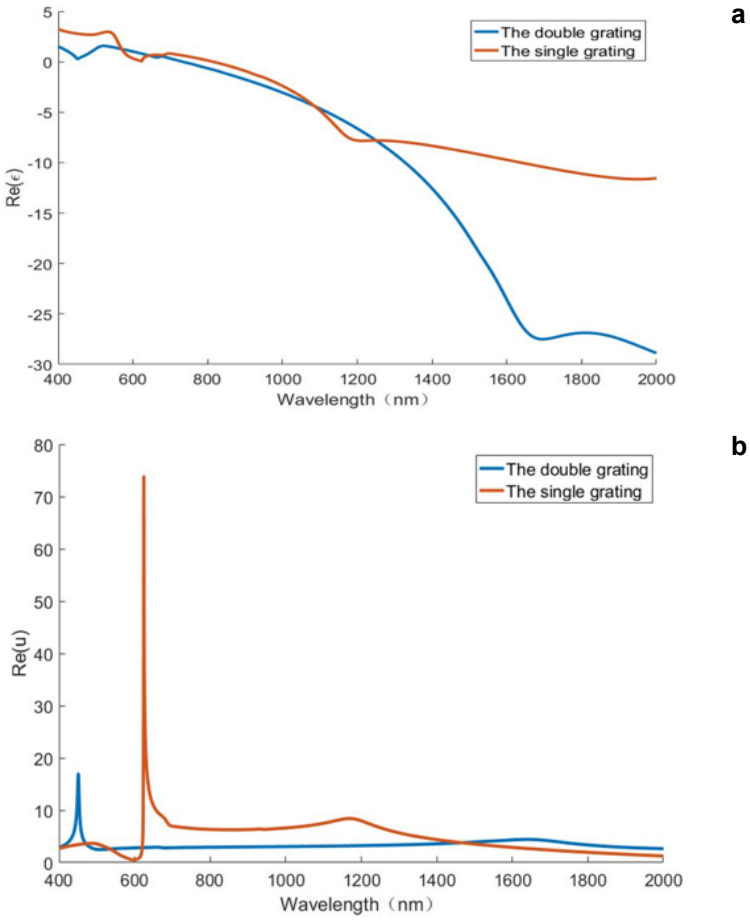

Fig. 9. Comparison of the effective constitutive parameters of designed metamaterial for single grating structure and double grating structure, respectively. (**a**) The effective permittivity, (**b**) the effective permeability, (**c**) the effective refractive index.

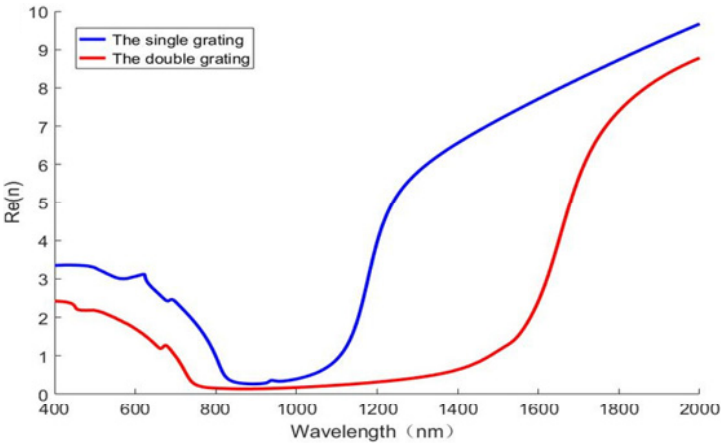

Fig. 9. Continued.

in the infrared band. Compared with the single grating structure, the resonance frequency of the double grating structure is redshifted. The effective permeability is shown in Fig. 9**b**. The resonant frequency interval of double grating is larger than that of single grating. The effective permeability of the double grating is less than that of the single grating at the higher order mode resonance frequency.

Figure 9**c** shows the effective refractive index for the single grating and double grating, respectively. We find that the zero refractive index of the broadband appears for the double grating structure. When TM wave is incident, the low refractive index frequency band is widened by the double grating structure, because the original charge arrangement is interrupted by the double grating structure, and the field intensity at the short wavelength is weakened compared with the intensity of the single grating, so the low refractive index frequency band is widened. Figure 10 shows the effect of

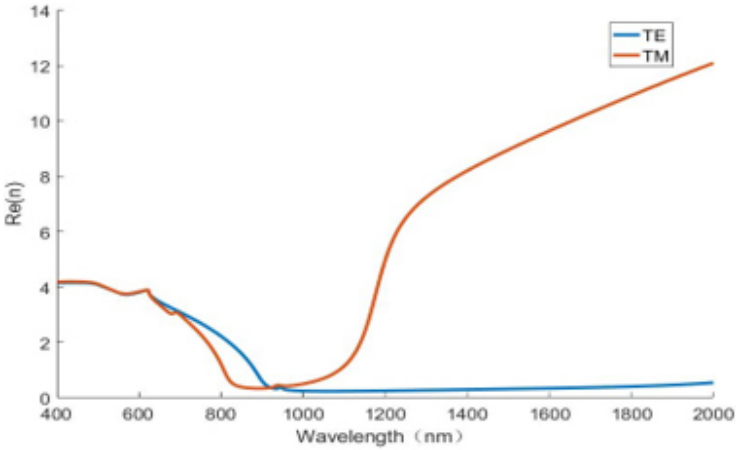

Fig. 10. Effect of different polarization on effective refractive index for double grating structure.

different polarization on effective refractive index for double grating structure. We find that the effect of different polarizations on the effective refractive index is similar to that of single gratings. When the incident light wave is in TE mode, the zero-refractive index characteristic of the broadband appears. In the same infrared frequency band, the metamaterial structure has a high refractive index when the incident light is in TM mode.

When $g = 10$ nm, $d = 40$ nm, and $t = 20$ nm, we further explore the effect of grating gap width h on the effective metamaterial parameters as shown in Fig. 11. With the decrease of grating gap h, the peak value of effective refractive index and dielectric constant increases continuously, and the resonance frequency at which the peak value is located shows a redshift phenomenon. The change of grating gap width h does not

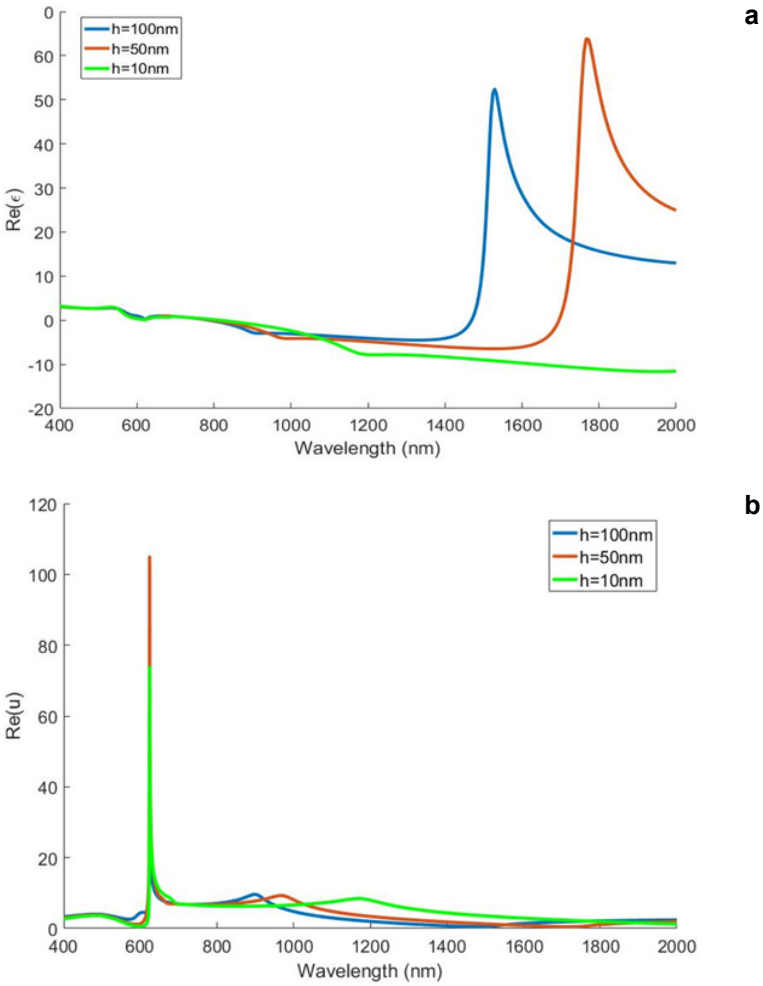

Fig. 11. Effect of gap width h of double grating on the effective constitutive parameters. (**a**) The effective permittivity, (**b**) the effective permeability, (**c**) the effective refractive index.

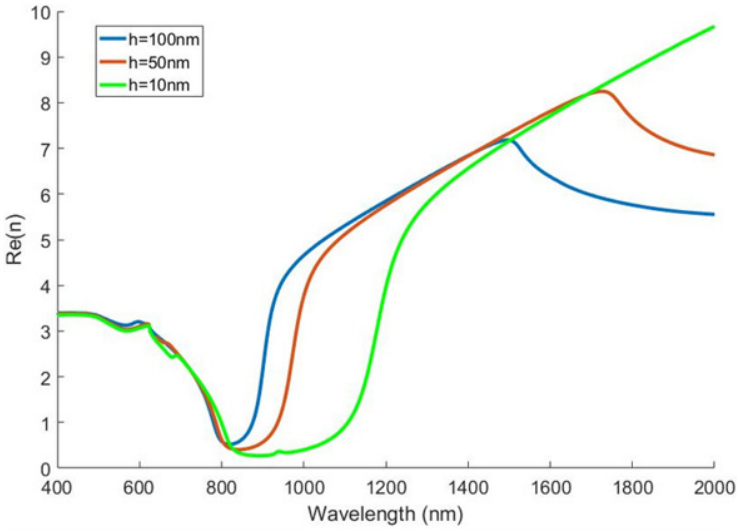

Fig. 11. Continued.

changes significantly the permeability. Compared with the single grating, the double grating metamaterial has an increased low frequency bandwidth.

To illustrate the physical properties of the double grating with the high refractive index, we calculated its near-field distribution as shown in Fig. 12. We find that the strong field region is concentrated in the grating grooves, and the near field of the double grating has penetrated into the substrate. Based on the principle of high refractive index metamaterial, the groove of the grating can be regarded as a capacitor. Due to the strong field, a large amount of charge accumulates inside the groove, resulting in the dipole momentum enhancement. Thus, the designed metamaterial structure has high refractive index properties at the resonance region.

Although our design focuses on numerical simulation, it is feasible to prepare the designed metamaterial gratings. A metal film is plated on the quartz substrate marked with cleaning treatment. Metal films can be prepared by magnetron sputtering. Then, a layer of photoresist is rotated on top of the metal film and baked. The structure model

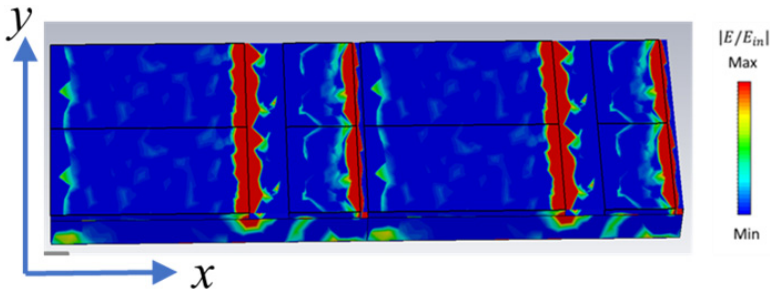

Fig. 12. Near-field distribution characteristic of double grating metamaterial.

of photoresist was prepared by electron beam exposure technique and then it was postbaked. After that, it is developed in the developer. Photoresist grating patterns were transferred to metal films by reactive ion etching. The photoresist is then removed. The entire preparation process can utilize this standard photolithographic preparation process.

6. Conclusions

In this paper, based on the principle of high refractive index metamaterials, a polarization sensitive grating structure which can realize effective high refractive index in infrared band is designed. Based on the capacitor between the grooves of the metal grating, the electric resonance response is enhanced and the effective dielectric constant of the metamaterial is improved. We reduce the diamagnetic effect of the metamaterial structure by reducing the thickness of the metal, thus increasing the permeability of the metamaterial. By changing the geometric parameters of the metal dielectric composite grating structure, the effective high refractive index of the metamaterial can reach more than 8.0. What is interesting is that when the incident light is at different polarization conditions, the metamaterial structure designed by us has both high refractive index and wide-band zero-refractive index properties. We further propose a double grating metamaterial structure to obtain more degrees of freedom of high refractive index metamaterial.

Acknowledgement
This work was supported by the National Key R&D Program of China (No. 2018YFF01013005); the National Natural Science Foundation of China (No. 52076200 and No. 62175224); the New-shoot Talents Program of Zhejiang province (No. 2021R409042 and No. 2021R409012); the Natural Science Foundation of Zhejiang Province (No. LZ21A040003, No. LY20F050007).

References

[1] Xiaoyong He, Feng Liu, Fangting Lin, Wangzhou Shi, *Tunable terahertz Dirac semimetal metamaterials*, Journal of Physics D: Applied Physics **54**(23), 2021, article ID 235103, DOI: 10.1088/1361-6463/abe898.

[2] Jun Peng, Xiaoyong He, Chenyuyi Shi, Jin Leng, Fangting Lin, Feng Liu, Hao Zhang, Wangzhou Shi, *Investigation of graphene supported terahertz elliptical metamaterials*, Physica E **124**, 2020, article ID 114309, DOI: 10.1016/j.physe.2020.114309.

[3] Xiaoyong He, Feng Liu, Fangting Lin, Wangzhou Shi, *Tunable 3D Dirac-semimetals supported mid-IR hybrid plasmonic waveguides*, Optics Letters **46**(3), 2021, pp. 472–475, DOI: 10.1364/OL.415187.

[4] He X., Zhong X., Lin F., Shi W., *Investigation of graphene assisted tunable terahertz metamaterials absorber*, Optical Materials Express **6**(2), 2016, pp. 331–342, DOI: 10.1364/OME.6.000331.

[5] Junxiang Huang, Tao Fu, Haiou Li, Zhaoyu Shou, Xi Gao, *A reconfigurable terahertz polarization converter based on metal–graphene hybrid metasurface*, Chinese Optics Letters **18**(1), 2020, article ID 013102, DOI: 10.3788/COL202018.013102.

[6] Teng S., Zhang Q., Wang H., Liu L., Lv H., *Conversion between polarization states based on metasurface*, Photonics Research **7**(3), 2019, pp. 246–250, DOI: 10.1364/PRJ.7.000246.

[7] AKRAM M.R., DING G., CHEN K., FENG Y., ZHU W., *Ultra-thin single layer metasurfaces with ultra -wideband operation for both transmission and reflection*, Advanced Materials **32**(12), 2020, article ID 1907308, DOI: 10.1002/adma.201907308.

[8] ZHANG J., WEI X., RUKHLENKO I.D., CHEN H.-T., ZHU W., *Electrically tunable metasurface with independent frequency and amplitude modulations*, ACS Photonics **7**(1), 2020, pp. 265–271, DOI: 10.1021/acsphotonics.9b01532.

[9] LIN LI, QUAN YUAN, RUN CHEN, XIUJUAN ZOU, WENBO ZANG, TIANYUE LI, GAIGE ZHENG, SHUMING WANG, ZHENLIN WANG, SHINING ZHU, *Chromatic dispersion manipulation based on metasurface devices in the mid-infrared region*, Chinese Optics Letters **18**(1), 2020, article ID 082401, DOI: 10.3788/COL202018.082401.

[10] BO FANG, ZHIYU CAI, YANDONG PENG, CHENXIA LI, ZHI HONG, XUFENG JING, *Realization of ultrahigh refractive index in terahertz region by multiple layers coupled metal ring metamaterials*, Journal of Electromagnetic Waves and Applications **33**(11), 2019, pp. 1375–1390, DOI: 10.1080/09205071.2019.1608868.

[11] FANG B., LI B., PENG Y., LI C., HONG Z., JING X., *Polarization-independent multiband metamaterials absorber by fundamental cavity mode of multilayer microstructure*, Microwave and Optical Technology Letters **61**(10), 2019, pp. 2385–2391, DOI: 10.1002/mop.31890.

[12] WEIMIN WANG, XUFENG JING, JINGYIN ZHAO, YINYAN LI, YING TIAN, *Improvement of accuracy of simple methods for design and analysis of a blazed phase grating microstructure*, Optica Applicata **47**(2), 2017, pp. 183–198, DOI: 10.5277/oa170202.

[13] LI JIANG, BO FANG, ZHIGANG YAN, CHENXIA LI, JIPENG FU, HAIYONG GAN, ZHI HONG, XUFENG JING, *Improvement of unidirectional scattering characteristics based on multiple nanospheres array*, Microwave and Optical Technology Letters **62**(6), 2020, pp. 2405–2414, DOI: 10.1002/mop.32328.

[14] JUNYU XIAO, RUIWEN XIAO, RONGXUAN ZHANG, ZHIXIONG SHEN, WEI HU, LEI WANG, YANQING LU, *Tunable terahertz absorber based on transparent and flexible metamaterial*, Chinese Optics Letters **18**(9), 2020, article ID 092403, DOI: 10.3788/COL202018.092403.

[15] OBULKASIM OLUGH, ZI-LIANG LI, BAI-SONG XIE, *Asymmetric pulse effects on pair production in polarized electric fields*, High Power Laser Science and Engineering **8**(4), 2020, article ID E38, DOI: 10.1017/hpl.2020.36.

[16] LEI XIA, YUANZHANG HU, WENYU CHEN, XIAOGUANG LI, *Decoupling of the position and angular errors in laser pointing with a neural network method*, High Power Laser Science and Engineering **8**(3), 2020, article ID E28, DOI: 10.1017/hpl.2020.29.

[17] HORNUNG J., ZOBUS Y., BOLLER P., BRABETZ C., EISENBARTH U., KÜHL T., MAJOR ZS., OHLAND J.B., ZEPF M., ZIELBAUER B., BAGNOUD V., *Enhancement of the laser-driven proton source at PHELIX*, High Power Laser Science and Engineering **8**(2), 2020, article ID E24, DOI: 10.1017/hpl.2020.23.

[18] FEI DING, YITING CHEN, BOZHEVOLNYI S.I., *Gap-surface plasmon metasurfaces for linear-polarization conversion, focusing, and beam splitting*, Photonics Research **8**(5), 2020, pp. 707–714, DOI: 10.1364/PRJ.386655.

[19] XUEQIAN ZHANG, QUAN XU, LINGBO XIA, YANFENG LI, JIANQIANG GU, ZHEN TIAN, CHUNMEI OUYANG, JIAGUANG HAN, WEILI ZHANG, *Terahertz surface plasmonic waves: a review*, Advanced Photonics **2**(1), 2020, article ID 014001, DOI: 10.1117/1.AP.2.1.014001.

[20] ZHANG J., ZHANG H., YANG W., CHEN K., WEI X., FENG Y., JIN R., ZHU W., *Dynamic scattering steering with graphene-based coding metamirror*, Advanced Optical Materials **8**(19), 2020, article ID 2000683, DOI: 10.1002/adom.202000683.

[21] BAI X., KONG F., SUN Y., WANG G., QIAN J., LI X., CAO A., HE C., LIANG X., JIN R., ZHU W., *High -efficiency transmissive programmable metasurface for multimode OAM generation*, Advanced Optical Materials **8**(17), 2020, article ID 2000570, DOI: 10.1002/adom.202000570.

[22] JING X., GUI X., ZHOU P., HONG Z., *Physical explanation of Fabry–Pérot cavity for broadband bilayer metamaterials polarization converter*, Journal of Lightwave Technology **36**(12), 2018, pp. 2322–2327, DOI: 10.1109/JLT.2018.2808339.

[23] Xia R., Jing X., Gui X., Tian Y., Hong Z., *Broadband terahertz half-wave plate based on anisotropic polarization conversion metamaterials*, Optical Materials Express **7**(3), 2017, pp. 977–988, DOI: 10.1364/OME.7.000977.

[24] Akram M.R., Mehmood M.Q., Bai X., Jin R., Premaratne M., Zhu W., *High efficiency ultrathin transmissive metasurfaces*, Advanced Optical Materials **7**(11), 2019, article ID 1801628, DOI: 10.1002/adom.201801628.

[25] Akram M.R., Bai X., Jin R., Vandenbosch G.A.E., Premaratne M., Zhu W., *Photon spin Hall effect-based ultra-thin transmissive metasurface for efficient generation of OAM waves*, IEEE Transactions on Antennas and Propagation **67**(7), 2019, pp. 4650–4658, DOI: 10.1109/TAP.2019.2905777.

[26] Zhao J., Jing X., Wang W., Tian Y., Zhu D., Shi G., *Steady method to retrieve effective electromagnetic parameters of bianisotropic metamaterials at one incident direction in the terahertz region*, Optics & Laser Technology **95**, 2017, pp. 56–62, DOI: 10.1016/j.optlastec.2017.04.001.

[27] Tian Y., Jing X., Gan H., Li C., Hong Z., *Free control of far-field scattering angle of transmission terahertz wave using multilayer split-ring resonators' metasurfaces*, Frontiers of Physics **15**, 2020, article ID 62502, DOI: 10.1007/s11467-020-1013-1.

[28] Fu Y., Fei Y., Dong D., Liu Y., *Photonic spin Hall effect in PT symmetric metamaterials*, Frontiers of Physics **14**, 2019, article ID 62601, DOI: 10.1007/s11467-019-0938-8.

[29] Fu Y., Tao J., Song A., Liu Y., Xu Y., *Controllably asymmetric beam splitting via gap-induced diffraction channel transition in dual-layer binary metagratings*, Frontiers of Physics **15**, 2020, article ID 52502, DOI: 10.1007/s11467-020-0968-2.

[30] Shen Z., Yang H., Liu X., Huang X., Xiang T., Wu J., Chen W., *Electromagnetically induced transparency in novel dual-band metamaterial excited by toroidal dipolar response*, Frontiers of Physics **15**, 2020, article ID 12601, DOI: 10.1007/s11467-019-0928-x.

[31] Li J., Jin R., Geng J., Liang X., Wang K., Premaratne M., Zhu W., *Design of a broadband metasurface Luneburg lens for full-angle operation*, IEEE Transactions on Antennas and Propagation **67**(4), 2019, pp. 2442–2451, DOI: 10.1109/TAP.2018.2889006.

[32] Lu X., Zeng X., Lv H., Han Y., Mou Z., Liu C., Wang S., Teng S., *Polarization controllable plasmonic focusing based on nanometer holes*, Nanotechnology **31**(13), 2020, article ID 135201, DOI: 10.1088/1361-6528/ab62d0.

[33] Lv H., Lu X., Han Y., Mou Z., Zhou C., Wang S., Teng S., *Metasurface cylindrical vector light generators based on nanometer holes*, New Journal of Physics **21**, 2019, article ID 123047, DOI: 10.1088/1367-2630/ab5f44.

[34] Lv H., Lu X., Han Y., Mou Z., Teng S., *Multifocal metalens with a controllable intensity ratio*, Optics Letters **44**(10), 2019, pp. 2518–2521, DOI: 10.1364/OL.44.002518.

[35] Wang H., Liu L., Zhou C., Xu J., Zhang M., Teng S., Cai Y., *Vortex beam generation with variable topological charge based on a spiral slit*, Nanophotonics **8**(2), 2019, pp. 317–324, DOI: 10.1515/nanoph-2018-0214.

[36] Jing X., Jin S., Tian Y., Liang P., Dong Q., Wang L., *Analysis of the sinusoidal nanopatterning grating structure*, Optics & Laser Technology **48**, 2013, pp. 160–166, DOI: 10.1016/j.optlastec.2012.10.008.

[37] Jing X., Xu Y., Gan H., He Y., Hong Z., *High refractive index metamaterials by using higher order modes resonances of hollow cylindrical nanostructure in visible region*, IEEE Access **7**, 2019, pp. 144945–144956, DOI: 10.1109/ACCESS.2019.2945119.

[38] Jiang L., Fang B., Yan Z., Fan J., Qi C., Liu J., He Y., Li C., Jing X., Gan H., Hong Z., *Terahertz high and near-zero refractive index metamaterials by double layer metal ring microstructure*, Optics & Laser Technology **123**, 2020, article ID 105949, DOI: 10.1016/j.optlastec.2019.105949.

[39] Xiao S., Drachev V., Kildishev A., Ni X., Chettiar U., Yuan H., Shalaev V., *Loss-free and active optical negative-index metamaterials*, Nature **466**, 2010, pp. 735–738, DOI: 10.1038/nature09278.

[40] KARALIS A., LIDORIKIS E., IBANESCU M., JOANNOPOULOS J.D., SOLJAČIĆ M., *Surface-plasmon-assisted guiding of broadband slow and subwavelength light in air*, Physical Review Letters **95**(6), 2005, article ID 063901, DOI: 10.1103/PhysRevLett.95.063901.

[41] HE Y., HE S., GAO J., YANG X., *Nanoscale metamaterial optical waveguides with ultrahigh refractive indices*, Journal of the Optical Society of America B **29**(9), 2012, pp. 2559–2566, DOI: 10.1364/JOSAB.29.002559.

[42] HADI TEGUH YUDISTIRA, AYODYA PRADHIPTA TENGGARA, VU DAT NGUYEN, TEUN TEUN KIM, FARIZA DIAN PRASETYO, CHOON-GI CHOI, MUHAN CHOI, DOYOUNG BYUN, *Fabrication of terahertz metamaterial with high refractive index using high-resolution electrohydrodynamic jet printing*, Applied Physics Letters **103**(21), 2013, article ID 211106, DOI: 10.1063/1.4832197.

[43] CAMPBELL T., HIBBINS A.P., SAMBLES J.R., HOOPER I.R., *Broadband and low loss high refractive index metamaterials in the microwave regime*, Applied Physics Letters **102**(9), 2013, article ID 091108, DOI: 10.1063/1.4794088.

[44] TAN S., YAN F., SINGH L., CAO W., XU N., HU X., SINGH R., WANG M., ZHANG W., *Terahertz metasurfaces with a high refractive index enhanced by the strong nearest neighbor coupling*, Optics Express **23**(22), 2015, pp. 29222–29230, DOI: 10.1364/OE.23.029222.

[45] LIU Z., ZHANG C., SUN S., YI N., GAO Y., SONG Q., XIAO S., *Polarization-independent metamaterial with broad ultrahigh refractive index in terahertz region*, Optical Materials Express **5**(9), 2015, pp. 1949–1953, DOI: 10.1364/OME.5.001949.

[46] SIEVENPIPER D.F., YABLONOVITCH E., WINN J.N., FAN S., VILLENEUVE P.R., JOANNOPOULOS J.D., *3D metallo-dielectric photonic crystals with strong capacitive coupling between metallic islands*, Physical Review Letters **80**(13), 1998, pp. 2829–2832, DOI: 10.1103/PhysRevLett.80.2829.

[47] SHIN J., SHEN J.T., FAN S., *Three-dimensional metamaterials with an ultrahigh effective refractive index over a broad bandwidth*, Physical Review Letters **102**(9), 2009, article ID 093903, DOI: 10.1103/PhysRevLett.102.093903.

[48] CHOI M., LEE S.H., KIM Y., KANG S.B., SHIN J., KWAK M.H., KANG K.Y., LEE Y.H., PARK N., MIN B., *A terahertz metamaterial with unnaturally high refractive index*, Nature **470**, 2011, pp. 369–373, DOI: 10.1038/nature09776.

[49] SMITH D.R., VIER D.C., KOSCHNY TH., SOUKOULIS C.M., *Electromagnetic parameter retrieval from inhomogeneous metamaterials*, Physical Review E **71**(3), 2005, article ID 036617, DOI: 10.1103/PhysRevE.71.036617.

[50] MIAN JIA, HUIHUI ZHU, DONGSHUO ZHU, WEIMIN WANG, GUOHUA SHI, XUFENG JING, *Highly efficient anomalous reflection by ultrathin phase gradient planar meta-surface arrays in near infrared region*, Optoelectronics and Advanced Materials – Rapid Communications **11**(3–4), 2017, pp. 148–152.

Received August 13, 2021
in revised form September 13, 2021